Analog Retinal Redshifts Visible Absorption of QuasAr Transmembrane Voltage Sensors into Near-infrared

Mei, G.X.; Mamaeva, N.; Ganapathy, S.; Wang, P.; Grip, W.J. de; Rothschild, K.J.

Analog Retinal Redshifts Visible Absorption of QuasAr Transmembrane Voltage Sensors into Near-infrared

Gaoxiang Mei[1], Natalia Mamaeva[1], Srividya Ganapathy[2] (iD), Peng Wang[3], Willem J. DeGrip[2,4] and Kenneth J. Rothschild*[1]

[1]Molecular Biophysics Laboratory, Photonics Center and Department of Physics, Boston University, Boston, MA
[2]Department of Biophysical Organic Chemistry, Leiden Institute of Chemistry,Leiden University, Leiden, The Netherlands
[3]Bruker Corporation, Billerica, MA
[4]Department of Biochemistry, Radboud Institute for Molecular Life Sciences,Radboud University Medical Center, Nijmegen, The Netherlands

ABSTRACT

Opsin-based transmembrane voltage sensors (OTVSs) are increasingly important tools for neuroscience enabling neural function in complex brain circuits to be explored in live, behaving animals. However, the visible wavelengths required for fluorescence excitation of the current generation of OTVSs limit optogenetic imaging in the brain to depths of only a few mm due to the strong absorption and scattering of visible light by biological tissues. We report that substitution of the native A1 retinal chromophore of the widely used QuasAr1/2 OTVSs with the retinal analog MMAR containing a methylamino-modified dimethylphenyl ring results in over a 100-nm redshift of the maxima of the absorption and fluorescence emission bands to near 700 and 840 nm, respectively. FT-Raman spectroscopy reveals that at pH 7 QuasAr1 with both the A1 and MMAR chromophores possess predominantly an all-*trans* protonated Schiff base configuration with the MMAR chromophore exhibiting increased torsion of the polyene single-/double-bond system similar to the O-intermediate of the BR photocycle. In contrast, the A1 and the MMAR chromophores of QuasAr2 exist partially in a 13-*cis* PSB configuration. These results demonstrate that QuasArs containing the MMAR chromophore are attractive candidates for use as NIR-OTVSs, especially for applications such as deep brain imaging.

INTRODUCTION

The Cohen laboratory first demonstrated in 2011 that the D97N mutant of the eubacterial light-driven proton pump green proteorhodopsin (GPR), termed PROPS, could be used as a fluorescent opsin transmembrane voltage sensor (OTVS) (1). In subsequent work, it was shown that the homologous D95N mutant of archaerhodopsin3 (AR3-D95N), the light-driven proton

pump found in the archaebacterium *Halorubrum sodomense,* can also function as a fluorescent OTVS (2). AR3-D95N absorbs maximally at 590 nm and fluoresces near 720 nm with the fluorescence intensity increasing with less negative transmembrane potential (*e.g.* such as when the nerve membrane is depolarized). Importantly, unlike GPR and its OTVS variants, AR3 and variants express well in animal cells. As a consequence, AR3-based OTVSs have facilitated a variety of functional neural imaging studies in living animals as well as studies aimed at understanding the basis for neurodegenerative diseases (3,4).

More recently, the application of directed evolution, such as based on hierarchal screening, has led to improved AR3-OTVSs such as QuasAr1 and QuasAr2 (Quality superior to Arch), which exhibit variable combinations of increased voltage sensitivity, brightness and photobleaching sensitivity (5). QuasAr1 and 2 contain five point-mutations in the AR3 sequence and differ only in the substitution of the native protonated Schiff base (SB) counterion (Asp95) with His95 (QuasAr1) or Gln95 (QuasAr2) (Fig. 1). QuasAr1 and QuasAr2 are much brighter than native AR3 under low-intensity illumination (15- and 3.3-fold, respectively). QuasAr1 exhibits the fastest time response (50 µs), while QuasAr2 exhibits the largest change in fluorescence in response to a change in membrane voltage. In addition, compared to ArcLight A242 (6), an engineered voltage sensor protein, QuasArs reported action potentials with 30- to 1000-fold better time resolution, although requiring 30-fold higher illumination intensity (5).

An important goal is to now develop OTVSs that both absorb and fluorescence in the NIR region (7,8). This is motivated by the high scattering and absorbance of visible light by most tissues including brain tissue, which prevents OTVSs from being used to optically monitor deep brain neural activity (*e.g.* below 2 mm in depth) without the use of invasive fiber optics. The development of OTVSs which excite and emit in the 650–950 nm optical transparency region would be particularly desirable since this is the region where light scattering and absorption by tissues is dramatically reduced (9). In addition, far-red absorbing OTVSs can avoid optical cross-talk with blue-green-light-activated ion gates such as channelrhodopsins used extensively in optogenetics (5,10–13).

In this study, we have focused on redshifting the excitation and fluorescence wavelength of QuasArs into the NIR as well as understanding the molecular basis for this extreme redshift in order to guide future bioengineering of NIR-OTVSs. Following
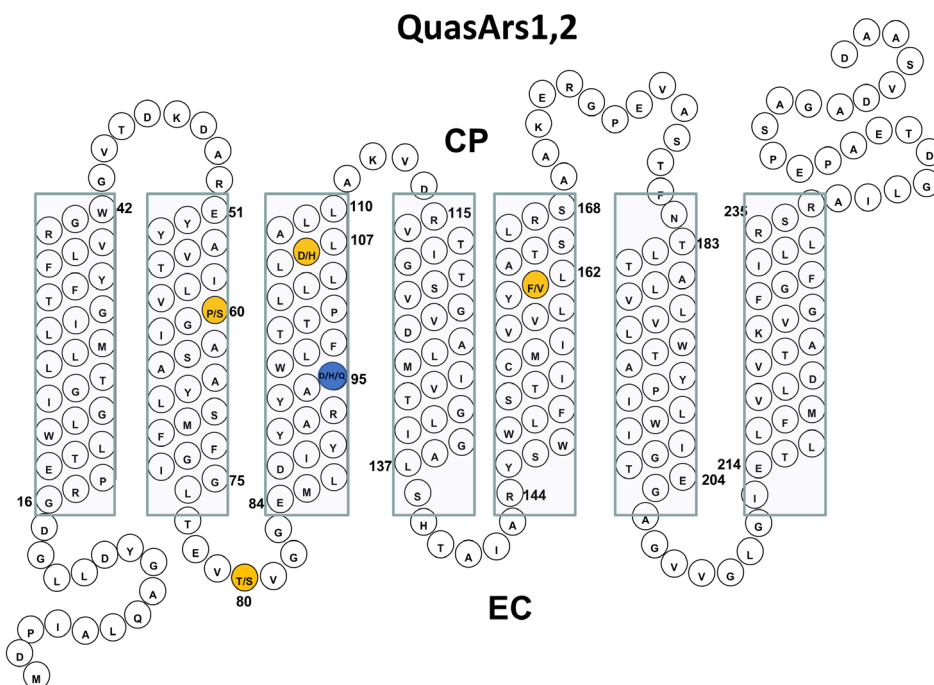

QuasArs1,2

Figure 1. Predicted 2D folding pattern of AR3 along with mutations in QuasAr1 and QuasAr2. Yellow circles show mutations P60S, T80S, D106H and F161V common to both QuasAr1 and QuasAr2. [Correction added on January 06, 2020, after first online publication: "F160V" was corrected to "F161V" in the previous sentence.] Blue circle shows mutation at the Schiff Base counterion D95: H95 for QuasAr1 and Q95 for QuasAr2 (5). [Correction added on January 06, 2020, after first online publication: In figure 1, the residue number near the residue L, adjacent to the third rectangle from the right was updated from 161 to 162.]

recent studies on the green proteorhodopsin (GPR) and its mutant D212N/F234S (14–16) and AR3 (17), we substituted the native retinal A1 chromophore in QuasAr1 and QuasAr2 with a retinal analog containing a methylamino substituted dimethylphenyl ring (MMAR) (see Figure S1). We find this results in a dramatic 100 nm redshift of the absorption maximum to near 700 nm, and a redshifted fluorescence emission to between 830 and 850 nm. Furthermore, compared to QuasAr1/2 with the native A1 chromophore, QuasAr1/2 containing the analog MMAR exhibit much brighter fluorescence. In contrast, a similar substitution of MMAR in the native AR3 and its mutant F229S, which is homologous to GPR-F234S, results in only 36 and 25 nm redshifts, respectively, but still generates a strong emission band centered around 815 nm (17). Preresonance FT-Raman reveals that in QuasAr1 both the A1 and the MMAR chromophore adopt an all-*trans* configuration with a protonated Schiff base (SB). However, the MMAR chromophore in addition exhibits increased torsion in the polyene single-/double-bond system similar to the late-stage O-intermediate of the BR photocycle. In contrast, in QuasAr2 the A1 and MMAR chromophore exist partially in a 13-*cis* configuration, which may correspond to an O-like 13-*cis* species observed in the photocycle of some BR mutants such as L93A. The MMAR chromophore in QuasAr2 again exhibits increased torsion in the polyene chain.

MATERIALS AND METHODS

Expression, purification and reconstitution of QuasArs with MMAR Retinal Analog. Methods for the expression, purification and reconstitution of QuasArs with both A1 and MMAR retinal in *E. coli* polar lipid membrane vesicles were similar to methods previously reported for wild type and variants of GPR with A1 and MMAR retinals

(15). pET 28b(+) vectors encoding QuasAr1 and QuasAr2 genes with a C-terminal His-tag were synthesized by GenScript (Piscataway, NJ). All-*trans* retinal was purchased from TRC company, Canada, and all-*trans* 3-methylamino-16-nor-1,2,3,4-didehydroretinal (MMAR; purity> 99.9%) was custom synthesized by Buchem, B.V., The Netherlands. Retinals were stored at −80°C in an ethanol stock solution. Octylglucoside (OG) and n-dodecyl-β-D-maltoside (DDM) were purchased from Anatrace Products, OH. Briefly, *E. coli (*strain BL21 (DH3), transformed with the pet28b(+) plasmid with the AR3, QuasAr1 or QuasAr2 genes) were grown in 0.5 L of LB medium with 50 mg L^{-1} kanamycin, to an O.D. of 0.4 at 600 nm at 35°C. All-*trans* retinal (2 μM) or all-*trans* MMAR (1 μM) and inducer (IPTG, 1 mM) were added, and cells were grown for an additional 4 h in the dark at 35°C. Cells were then harvested by centrifugation using a Beckman-Coulter Spinchron DLX tabletop centrifuge at 3000 RPM (~860 g), resuspended in sonication buffer (50 mM Tris, 5 mM MgCl$_2$ at pH 7.0) and lysed by freeze–thaw followed by sonication of the sample on ice for 1 min, 3 times. The lysate was then centrifuged at 38 000 RPM (~63 800g) with a Beckman-Coulter Optima L-90K ultracentrifuge with a 70 Ti rotor, and the pellet resuspended in binding buffer (20 mM HEPES, 150 mM NaCl,10 mM imidazole; pH 7.0). The mixture was homogenized with a glass Wheaton homogenizer, 2% OG or 2% DDM added, and incubated at 4°C overnight using a rotary shaker and again centrifuged for 30 min at 27 000 RPM (~32 000 *g*) using the Beckman-Coulter Optima L-90K ultracentrifuge. Nickel-chelated nitrilotriacetic acid (Ni-NTA) agarose beads (QIAGEN) were washed with the binding buffer, added to the supernatant and incubated 2 h at 4°C using a rotary shaker. Ni-NTA agarose beads with bound protein were loaded into 3 mL disposable plastic columns and washed with 5 mL of wash buffer (50 mM HEPES, 100 mM NaCl, 10 mM imidazole, 1% OG; pH 7.0). Protein was eluted with 1.5 mL of elution buffer (50 mM HEPES, 100 mM NaCl, 1% OG, 400 mM imidazole; pH 7.0 at room temperature). Purified His-tagged QuasAr pigments were reconstituted in *E. coli* polar lipids (ECPL) (Avanti, Alabaster AL) at 1:10 protein-to-lipid (w/w) ratio. Lipids were dissolved at 5mg mL^{-1} by sonication in binding buffer with 1% OG followed by filtration. The lipid solution was incubated with the OG-solubilized protein for 15 min at 4°C and dialyzed against the dialysis buffer (50 mM K$_2$HPO$_4$, 300 mM NaCl pH 7.0) overnight at 4°C followed by a buffer change and an additional dialysis for 3 h. The

reconstituted protein was centrifuged for 3 min at 15 000 rpm (21 000 g) and resuspended in 5 mM K_2HPO_4, 100 mM NaCl, pH 7.0 buffer three times consecutively. QuasAr samples were stored at 4°C.

UV-VIS-NIR absorption spectroscopy. The protein samples for absorption measurements were prepared as previously reported (18–20) using approximately 100 µg of the protein in the form of reconstituted ECPL lipid membranes as described above. The samples were washed followed by centrifugation at least three times in approximately 0.1 mL of buffer (pH 3 buffer: 5 mM NaH_2PO_4, 10 mM NaCl, 10 mM MES; pH 5 buffer: 5 mM NaH_2PO_4, 10 mM NaCl, 10 mM MES; pH 7.3 buffer: 50 mM NaCl, 5 mM HEPES; pH9.5 buffer: 50 mM NaCl, 10 mM CHES). After the final wash, the supernatant was removed, and the sample resuspended in 100 µL of the above-described buffer. The samples were then placed in a quartz cuvette (Thorlabs Inc., Newton, NJ). UV-Vis-NIR absorption measurements were performed at room temperature on a Cary 6000i instrument equipped with a diffuse reflectance accessory (DRA) (Agilent Technologies, Santa Clara, CA). The samples were scanned at a rate of 600 nm min^{-1} over the range of 200-900 nm.

Fluorescence spectroscopy. The protein samples used for fluorescence measurements were prepared in a similar manner to those previously described for absorption measurements except that the reconstituted membrane was dissolved in the detergent DDM. Approximately 50 µg of the reconstituted sample was spun in a SCILOGEX D3024 centrifuge at 15 000 rpm for 5 min, and the resulting pellet was washed at least three times in approximately 0.1 mL of buffer as described above for the different pH values. The final pellet was resuspended in 300 µL detergent solution (50 mM bis-tris-propane, 150 mM NaCl, 1 mM DTT and 2% DDM (w/v); pH 7). Fluorescence was measured using a Horiba NanoLog 3-22-TRIAX spectrofluorometer (HORIBA Jobin Yvon Inc., Edison, NJ) with a 450 W Xenon arc lamp excitation source, CCD detector and double monochromator on both the excitation and emission sides. The 300 µL samples were placed in the quartz cuvette and data collected with excitation wavelength from 450 nm to 706 nm and 0.1 s integration time. The collected data were corrected for lamp power and detector sensitivity. Relative brightness of the samples with excitation maxima at 600 nm was measured on the NanoLog fluorescence spectrometer and corrected for absorption of the identical samples measured using a Cary6000i absorption spectrometer equipped with a DRA (see above). Measurements of fluorescence emission were also made on QuasAr1:MR samples prepared in the same way as described below for FT-Raman measurements using a Renishaw inVia confocal Raman microscope equipped with 785-nm diode excitation, a CCD detector and a 20x objective with numerical aperture (NA) of 0.4. Fluorescence emission was measured at different power levels as indicated in Results.

Fourier transform Raman spectroscopy. Reconstituted QuasAr1 and QuasAr2 membrane vesicles with the A1 or MMAR chromophores were measured in aqueous buffer at different specific pHs in glass capillaries as described previously (21). Approximately 30 µg of the reconstituted sample was spun in a SCILOGEX D3024 centrifuge at ~ 21 000 g for 5 min, and the resulting pellet was resuspended in the same wash buffer as described above for the different pH values. The vesicles were then repelleted and washed at least 2 additional times to form a final pellet. This pellet was resuspended in a small amount of the wash buffer (<5 µL) and transferred using a 10 µL syringe (Hamilton Company, Reno, NV) to a 0.5-mm ID square borosilicate glass capillary (Fiber Optic Center, New Bedford, MA) with one end sealed. The capillary was spun at a lower speed (9500 g, 3 min), and then, the open side was sealed with Critoseal (Leica Microsystems, Buffalo Grove, IL).

FT-Raman measurements using 1064-nm laser excitation were obtained on a Bruker MultiRam FT-Raman spectrometer operating at 4 cm^{-1} resolution and power ranging from 30 to 300 mW. In addition to the 1064 cm^{-1} laser, diffuse scattered light from a low-power (~1 mW) HeNe laser used for calibration of the FT-interferometer mirror movement also irradiated the sample. An additional external light was used where indicated to further illuminate the sample consisting of an LED with emission peaking at 570 and 460 nm that is normally used as part of an alignment camera accessory for the Bruker MultiRam FT-Raman spectrometer.

Spectral analysis. Spectral subtractions, baseline corrections, Fourier self-deconvolution (FSD) and peak fitting were all performed using the data analysis programs provided in GRAMS/AI v7.02 data analysis suite (Thermo Fisher Scientific, Inc.). In order to baseline correct the absorption spectra for light scattering effects, the absorption in the 250-

850 nm region was corrected by interactively subtracting a quartic curve and normalizing spectral intensity to the protein band near 280 nm. This allowed comparison of the approximate wavelength of the main α-band characteristic of all rhodopsin pigments. Since this procedure may hide or distort contributions from smaller bands such as the β-band, also characteristic of rhodopsin pigments and normally located in the 350-400 nm range for A1 retinal pigments and closer to 500 nm for MMAR pigments (14,16,22), corresponding baseline uncorrected spectra are also shown which are again normalized using the intensity of the 280 nm protein peak. Fourier self-deconvolution (FSD) was performed on the FT-Raman spectra from 1415 to 1565 cm^{-1} with a γ-factor of 8 and 30% Bessel function smoothing. The FT-Raman spectra were first fit to a linear baseline and then curve-fitted in the 1415–1565 cm^{-1} region using an iterative χ-squared minimization program (provided with the GRAMS/A1 v7.02 suite). The initial peak positions were determined by FSD. This curve-fitting procedure, which uses a linear baseline correction, determined 9 Voigtian peaks for the QuasAr1:MR FT-Raman spectra from 1415 to 1565 cm^{-1}, which resulted in R^2 values better than 0.99. The same program was also used for curve fitting the UV-Vis spectrum in the range 450-850 nm with a Gaussian peak and a linear baseline to give an estimate of the bandwidth of the α-band.

Homology modeling. A homology model for QuasAr1 was constructed using the structure of BR as a template (PDB: 3HAR) (23), which has 57% sequence identity with AR3. Model building and subsequent analysis were performed using the WHAT IF (PMID:2268628) and YASARA (PMID:11948792) Twinset with standard parameters based on earlier work modeling AR3 (17).

RESULTS

Extreme redshifting of QuasAr absorption into the NIR

The baseline corrected absorption spectrum of AR3 and QuasAr1 with A1 retinal (AR3:A1 and QuasAr1:A1) reconstituted into ECPL lipid membranes (membrane vesicles) at pH 7.3 in the region 450-850 nm is shown in Fig. 2a. Compared to AR3:A1, the absorption maximum of QuasAr1:A1 exhibits a modest 28-nm redshift (from 560 nm to 588 nm). Although QuasAr1 has five point-mutations relative to native AR3, this redshift is most likely due almost entirely to substitution of a neutral His95 for a negatively charged Asp95 SB counterion at pH 7. In support of this, the AR3-D95N mutant also absorbs near 590 nm in ECPL reconstituted membranes due to the substitution of a negatively charged (Asp95) for a neutral (Asn95) residue (24).

In contrast to this modest redshift, substitution of the QuasAr1 A1 chromophore with the MMAR analog (QuasAr1:MR) (Figure S1) produces a dramatic ~ 100 nm redshift (588 to 688 nm) (Fig. 2a). The bandwidth (full width at half maximum; FWHM) also increases substantially from 106 to 169 nm based on a single component Gaussian curve fit. Significantly, this broadening extends the QuasAr1:MR absorption well into the NIR (>700 nm).

A similar extreme redshift and peak broadening is also observed upon substitution of the A1 chromophore of QuasAr2 (QuasAr2:A1) with MMAR (QuasAr2:MR) (Fig. 2b). In this case, the absorption maximum is at 705 nm with a bandwidth of 187 nm compared to 106 nm for QuasAr2:A1. Note the normal Asp95 SB counterion in AR3 is replaced in QuasAr2 with Gln95, which is expected to remain neutral like Asn over a wide pH range.

Since the data shown in Fig. 2a,b were measured from samples that were only dark-adapted for 10 minutes after exposure to ambient light, absorption spectra were also recorded from samples after overnight dark adaption (~12 hours) (Figure S2). These data are shown over the extended range 250-850 nm
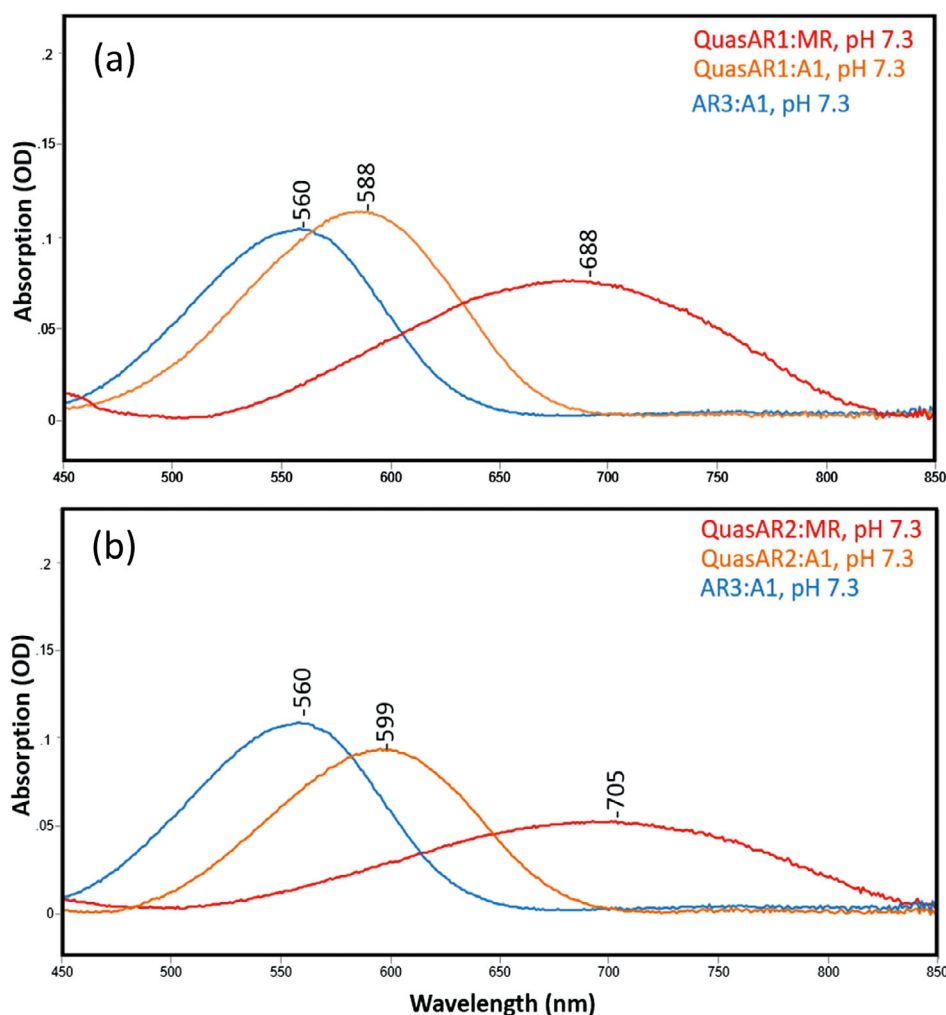
Figure 2. Comparison of absorption spectra from 450 to 850 nm of AR3 (blue trace) and different QuasArs reconstituted into ECPL lipid membrane vesicles at pH 7.3. (a) AR3 (blue trace), QuasAr1 with A1 retinal (orange trace) and MMAR (MR) (red trace). (b) AR3 (blue trace), QuasAr2 with A1 retinal (orange trace) and MMAR (MR) chromophores (red trace). All spectra were baseline corrected and scaled to the protein band at 280 nm (see Materials and Methods). Y-axis scale is for QuasAr1:MR (a) and QusAR2:A1 (b).

without baseline correction since this leads to distortion of the band shapes as discussed in the Methods section. Importantly, prolonged dark adaptation did not alter the position of the absorbance maximum of the major visible band (compare Fig. 2a,b to Figure S2). Other bands in Figure S2 are assigned to the protein aromatic groups (~280 nm) and *E. coli* cytochromes (414 nm) that tend to be copurified with his-tagged rhodopsins when using Ni-NTA agarose His-tag affinity chromatography for purification (22,25).

Since the absorption spectra in Fig. 2 were normalized to the 280 nm protein absorbance band, the molar absorbance of the MMAR pigments for the major visible-NIR band appears to be substantially smaller than that of the corresponding A1 pigments. This is in agreement with earlier studies on GPR:MR and GR:MR (*Gloeobacter* rhodopsin containing a MMAR chromophore), where it was found these pigments have molar absorbance coefficients about 60% of the corresponding A1 pigments ((14); Table S2 of reference). However, the possibility cannot be eliminated that the lower absorption is due at least in part to the lower thermal stability of MMAR pigments in detergent solution (14). For example, some pigment could be lost during purification of

the MMAR containing QuasArs. Alternatively, incomplete regeneration by MMAR of the QuasArs expressed in *E. coli* could also result in such an effect.

Extreme redshifting of the fluorescence of QuasArs into the NIR

Excitation/emission measurements were performed on QuasAr1/2:A1 solubilized in DDM micelles. The fluorescence spectra with excitation at 600 nm (Fig. 3), near the absorption maxima of these pigments, exhibit fluorescence emission peaking at 715 and 730 nm for QuasAr1:A1 and QuasAr2:A1, respectively, in agreement with earlier measurements (5). Contour plots of the emission vs. excitation (Figure S3A,C) reveal that the wavelength of maximum excitation falls close to the absorption maximum. Note that both the absorption and excitation maxima of QuasAr2:A1 are redshifted slightly compared to QuasAr1:A1 (Fig. 3 and Figure S3).

In contrast to QuasArs with A1 retinal chromophores, QuasArs containing the MMAR chromophore (QuasAr1/2:MR) when excited near their absorption maxima (690 nm) exhibit a
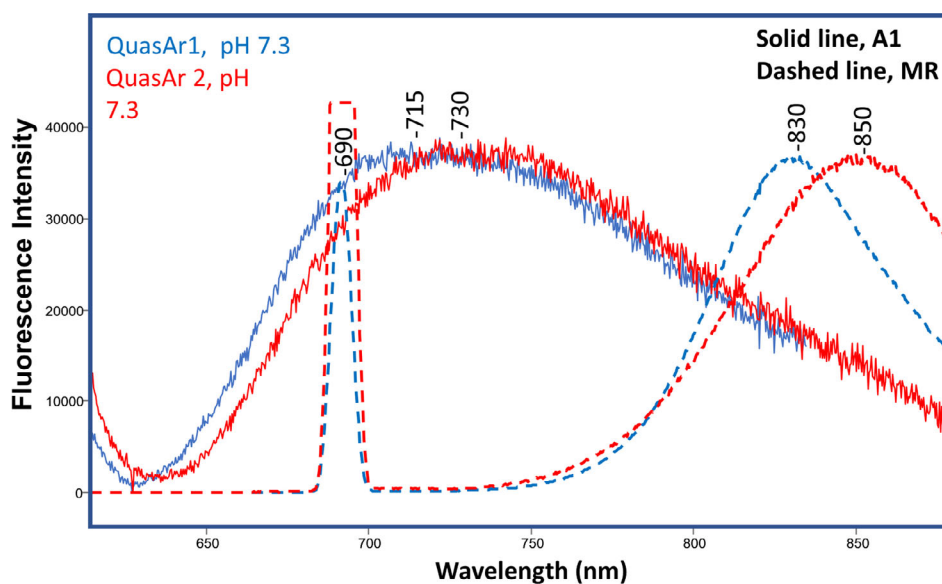
Figure 3. Fluorescence spectra of QuasArs in DDM micelles at pH 7.3 from 600 to 900 nm. Solid traces are for QuasArs with A1 retinal chromophore and dashed traces for QuasArs with MMAR chromophore. QuasAr1 is shown as blue trace, and QuasAr2 is shown as red trace. Peak excitation wavelength for QuasArs with A1 chromophore was 600 nm and for QuasArs with MMAR chromophore 690 nm. Y-axis shown is for QuasAr2 with MMAR chromophore, and the emission bands are normalized to the QuasAr2:MR band. The peak at 690 nm is an artifact due to scattering of excitation at 690 nm used for the QuasArs with MMAR chromophore.

large ~ 100 nm redshift of the fluorescence maxima (Fig. 3), which is relatively independent of the exciting wavelength based on the contour plots (Figure S3). Furthermore, the bandwidths of the QuasAR1/2:MR emission bands are much smaller than for QuasAr1/2:A1. Although absolute measurements of the quantum yield of QuasaAR1/2:MR were not made, the current measurements indicate that QuasAr1/2:MR analogs are much brighter than the corresponding QuasAr1/2:A1. For example, even when all the samples are excited with the same intensity 600 nm light, *close to the excitation maximum of QuasAr1,2:A1* and when the pigment concentration and an approximately 50% smaller extinction coefficient are taken into account (see above), *the QuasAr1,2:MR samples still fluoresce much brighter by a factor of approximately 5x and 10x, respectively* (Figure S4).

Fluorescence emission was also measured for QuasAr1:MR with 785 nm NIR laser excitation using a confocal Raman microscope (see Materials and Methods) (Figure S5). Although resonance-enhanced Raman peaks could not be detected due to the extremely high fluorescence emission compared for example to QuasAr1:A1, the fluorescence profiles over the limited range 830 to 915 nm could be measured even at low power. In agreement with the above fluorescence measurements using 600 and 690 nm excitation, the emission peaks are extremely redshifted compared to QuasAr1:A1 over 100 nm. In addition, the intensity is linear for QuasAR1:A1 over a five-fold range of excitation power (0.5 to 2.5 μW) up to where the detector was saturated due to brightness.

FT-Raman reveals chromophore configuration of QuasArs with MMAR chromophore

QuasAr1:A1/MR. FT-Raman spectroscopy using 1064-nm excitation preferentially enhances the vibrational spectrum of the retinylidene chromophore of microbial rhodopsins over protein

vibrations due to preresonance effects (15,26–28). In addition, the 1064-nm excitation avoids interference from the strong fluorescence band at 750-950 nm in the case of QuasAr1/2:MR (Figure S3A–D). The FT-Raman spectrum of QuasAr1:A1 measured at pH 7.3 (Fig. 4a, red trace) is similar to redshifted microbial rhodopsins with all-*trans* retinylidene protonated SB chromophores (all-*trans* retinal PSB). For example, an intense band appears at 1518 cm^{-1} in the ethylenic (C=C stretch) region, which along with the measured λ_{max} at 588 nm (Fig. 2a) falls close to the linear correlation observed between $\nu_{C=C}$ and λ_{max} for microbial rhodopsins (15,18,21,29–31) (Figure S6, blue dot on dashed green line). In fact, QuasAr1:A1 falls very close to sensory rhodopsin I (1520 cm^{-1}, 587 nm), which has an all-*trans* retinylidene protonated SB with a neutral counterion (Asp76) at pHs below 7 (32–34). In addition, the configurationally sensitive C-C stretch fingerprint region from 1100 to 1250 cm^{-1} is similar to other microbial rhodopsins with an all-*trans* retinal PSB chromophore such as BR, AR3 (AR3:A1) (24) and SRI (32). Most prominent are the bands at 1199 and 1168 cm^{-1} assigned in analogy with BR to the localized C$_{14}$-C$_{15}$ and C$_{10}$-C$_{11}$ retinal stretching modes, respectively (18,35–37). The lower ratio of the 1199/1168 cm^{-1} band intensity compared to BR and AR3 most likely reflects the pigment's redshifted λ_{max} similar to the lower ratio observed in the resonance Raman spectrum of the O-intermediate of the BR photocycle (38). A band appearing at 1653 cm^{-1} in the SB C=N-H stretching region is consistent with its assignment to a protonated Schiff base (37,39). However, since this band appears at a higher frequency compared to similarly assigned bands in BR (1639 cm^{-1}), AR3 (1641 cm^{-1}) (24) and especially SRI (1628 cm^{-1}) (32), we cannot exclude the possibility that this band arises from or contains contributions from the intense water band near 1650 cm^{-1} and/or the Amide I vibration from the opsin protein backbone, which appears between 1650 and

1660 cm^{-1} for animal rhodopsins (40) and microbial rhodopsins (41). A weak band also appears in the hydrogen-out-of-plane (HOOP) region at 967 cm^{-1} close to the frequency assigned to the coupled HOOP mode in AR3 (959 cm^{-1}) and BR (958 cm^{-1}) (24). The weak intensity of this band indicates that unlike the O-intermediate of BR, little torsion exists in the polyene chain of ground-state QuasAr1:A1.

The FT-Raman spectra of QuasAr1:MR measured at pH 3, 5, 7.3 and 9.5 are also shown in Fig. 4a (blue, orange, green traces,

respectively). In the pH range 5-9.5, the spectra are largely insensitive to pH in contrast to the cases of GPR:MR and GPR-DNFS:MR, where a significant pH dependence was reported (15,16). This is most likely due to the presence in these cases of an Asp counterion, the charge of which is pH-dependent (see also discussion in ref. 17). Furthermore, the spectra are similar to QuasAr1:A1 with several notable exceptions. The ethylenic band has downshifted from 1518 to near 1515 cm^{-1}, which based on the correlation between λ_{max} and $\nu_{C=C}$ (Figure S6), would only
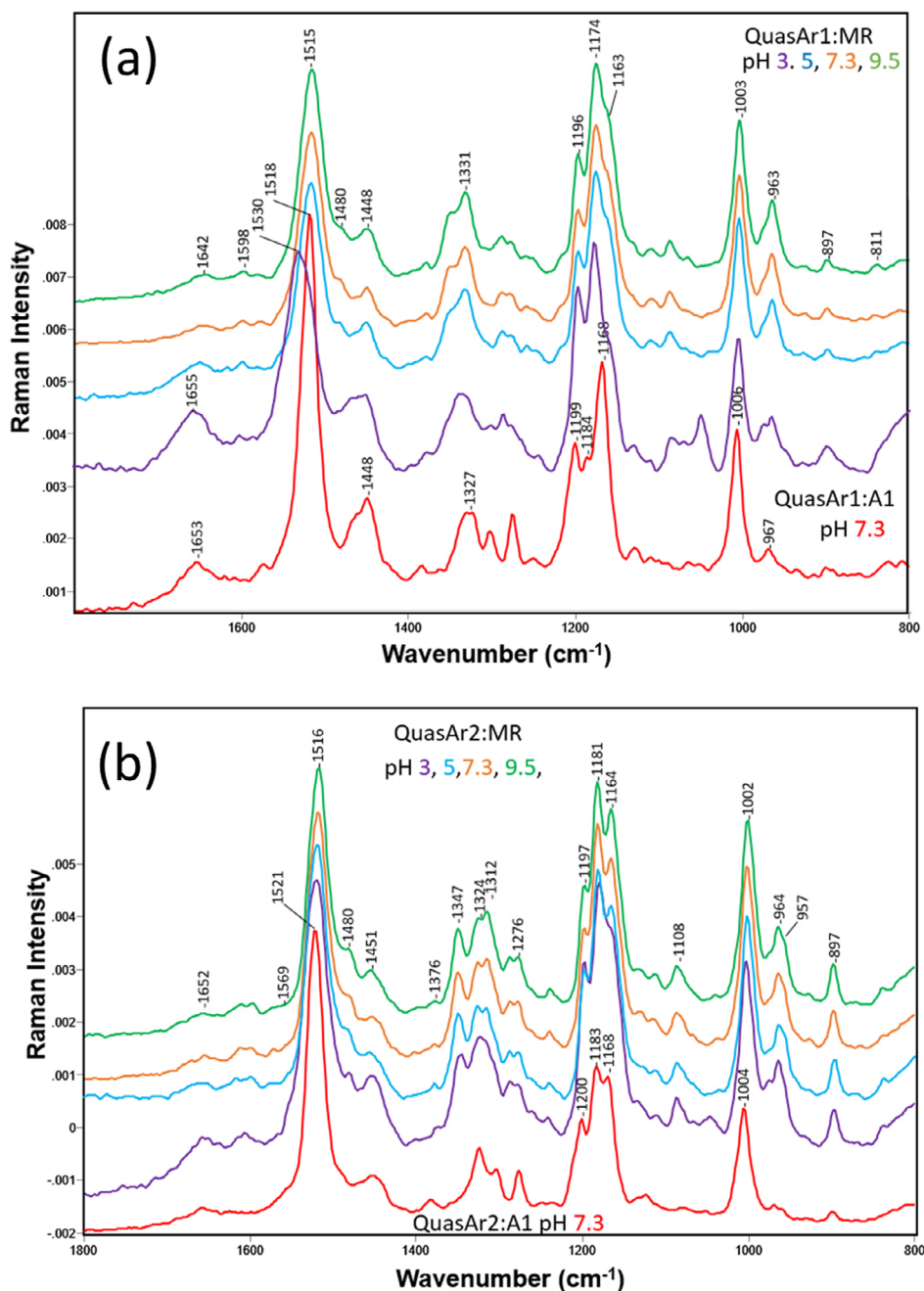

Figure 4. FT-Raman spectra of QuasArs in reconstituted membrane vesicles at different pHs. (a) QuasAr1 with the A1 chromophore at pH 7.3 (red), QuasAr1 with MMAR chromophore at pH 9.5 (green), 7.3 (orange), pH 5 (blue) and pH 3 (purple). Y-axis scale shown is for QuasAr1 with A1 chromophore. (b) QuasAr2 with the A1 chromophore at pH 7.3 (red), QuasAr2 with MMAR chromophore at pH 9.5 (green), 7.3 (orange), pH 5 (blue) and pH 3 (purple). Y-axis shows scale for QuasAr2 with MMAR at pH 9.5. All spectra were scaled using the band near 1003 cm^{-1}. Laser power was 300 mW for all samples, and data acquisition times varied between 1.9 and 10.8 h (see Materials and Methods for additional details).

produce an additional ~ 10–15 nm redshift in λ_{max}, far from the measured λ_{max} near 690 nm (Fig. 2a). However, the bandwidth of the ethylenic band is much broader compared to QuasAr1:A1 (Figure S7A), especially on the low-frequency side of the band. As discussed later, this may be due to increased structural variability of the MMAR chromophore in the QuasAr1 retinal binding pocket along with multiple resonance forms compared to A1. In earlier Raman studies of green proteorhodopsin and its mutant D212N/F234S with an MMAR chromophore (GPR:MR and GPR-DNFS:MR), similar broadening was observed with subcomponent bands appearing near 1498 and 1482 cm^{-1}, which were correlated to NIR-absorbing components beyond 700 nm (15,16). A curve fit of this region for QuasAr1:MR at pH 7.3 reveals several potential subcomponent bands (Figure S7B). Besides the major subcomponent band located near 1515 cm^{-1} (which predicts an absorption subcomponent band near 625 nm (red line, Figure S6)), additional subcomponents appear at 1527, 1504 and 1480 cm^{-1}, which would correspond to species absorbing near 580, 670 and 770 nm, respectively, on the basis of the $\nu_{C=C}$ vs. λ_{max} correlation established previously for subcomponent bands of GPR-DNFS:MR (Figure S6, red line with orange dots) (15). Interestingly, a similar pattern of subcomponent bands in both the FT-Raman and visible absorption is also observed in GPR-DNFS:MR (15) with subspecies absorbing at 563, 623, 708 and 781 nm. However, one difference is that in the case of QuasAr1:MR, the subcomponent band at 1515 cm^{-1} is the most intense even though the absorption spectrum indicates the more redshifted absorbing subcomponents are most dominant. The reason for this is presently unknown. However, one possibility is that the 625 nm absorbing subcomponent is more dominant under the conditions of the FT-Raman measurements compared to the absorption measurements.

In the fingerprint region (Fig. 4a), two bands appear at 1196 and 1174 cm^{-1} characteristic of an all-*trans* retinal configuration (18,35–37). Again, the lower ratio of the 1196/1174 cm^{-1} bands and shift in frequency compared to QuasAr1:A1 may reflect the redshifted chromophore and change in bond-length alteration along the conjugated chain of MMAR. In the coupled hydrogen-out-of-plane (HOOP) mode region, a band appears at 963 cm^{-1}, which is not far from the 967 cm^{-1} band in QuasAr1:A1 (Fig. 4a). However, the band is significantly increased in intensity compared to QuasAr1:A1, indicating increased torsion around the single- and double-bond system in the MMAR polyene chain (15,42–44). Additional weak bands are also detected at 897 and 811 cm^{-1}, which are most likely due to additional isolated HOOP modes. A band also appears in the protonated SB (-C=N-H stretching) region at 1642 cm^{-1} downshifted somewhat from QuasAr1:A1 and thus unlikely to have contributions from water or Amide I protein backbone vibrations.

Below pH 5, the FT-Raman spectrum of QuasAr1:MR changes considerably (Fig. 4a and Figure S7A, purple trace). Most notably, at pH 3 the ethylenic band undergoes a large upshift to 1530 cm^{-1} corresponding to a blueshift in absorption to near 560 nm based on the λ_{max} vs. $\nu_{C=C}$ correlation (Figure S6). The band assigned to the -C=N-H stretching also appears to upshift to 1655 cm^{-1} indicating a change in the environment near the SB region of the chromophore or increased contribution from water or Amide I modes. The C-C fingerprint region is still characteristic of an all-*trans* retinal chromophore with bands at 1196 and 1176 cm^{-1}. Furthermore, the frequency of most other bands in the spectrum (e.g. at 1334, 1004, 964 and

897 cm^{-1}) are largely unaltered relative to higher pH spectra. However, an increase in a band at 795 cm^{-1} (not shown) may indicate an increase in 13-*cis* isomer (see below). Further, the HOOP mode at 964 cm^{-1} decreases in intensity indicating less torsion around the single- and double-bond system of MMAR. Thus, as discussed later in more detail these results indicate that below pH 5 the His95 SB counterion in QuasAr1:MR becomes protonated with a net positive charge causing a blueshift in the absorption. In contrast, microbial rhodopsins with an Asp counterion become neutral at low pH and undergo a redshift.

QuasAr2:A1 and MR. Instead of the His95 PSB counterion in QuasAr1, QuasAr2 contains a Gln95 residue (Fig. 1). The FT-Raman spectrum of QuasAr2:A1 is quite similar to QuasAr1:A1 (Fig. 4b and Figure S8) except notably in the 1100–1250 cm^{-1} C-C stretch fingerprint region. An intense band appears at 1183 cm^{-1} characteristic of a 13-*cis* retinal configuration and assigned previously on basis of isotope substitution and normal mode calculations to the C_{10}-C_{11} stretching mode in the 13-*cis* polyene chain (45). For example, bands at a similar frequency appear in the N-intermediate of the BR photocycle, whose chromophore has a 13-*cis*, 15-*anti* configuration (46–48) and in dark-adapted BR where part of the chromophores has a 13-*cis*, 15-*syn* configuration (45). An additional indication that the QuasAr2:A1 chromophore at least partially adopts the 13-cis configuration is the appearance of a band at 795 cm^{-1} assigned to the C_{14} - H HOOP mode in dark-adapted BR (45) (Figure S9, blue trace). Since this band is somewhat broad, it may contain subcomponent bands. Note that no distinct bands of this intensity were detected in this region for the A1 and MR pigments of QuasAr1 (Figure S9), except at a pH below 5.

In the case of QuasAr2:MR, the overall spectrum is similar to QuasAr2:A1 with an intense band appearing at 1181 cm^{-1} characteristic of a 13-*cis* isomer as discussed above (Fig. 4b). In addition, a band appears at 795 cm^{-1} further supporting the existence of the 13-*cis* configuration (Figure S9). Like QuasAr1:MR, the FT-Raman spectrum does not change significantly in the pH range 9.5-5. However, in contrast to QuasAr1:MR, no significant shift in the ethylenic band frequency is seen at pH 3 (only a small shift occurs from 1516 to 1519 cm^{-1}), although the 1181 cm^{-1} band increases in intensity relative to the 1164 cm^{-1} potentially indicating a further increase in the 13-*cis* isomer content. Similar to QuasAr1:MR, the ethylenic band of QuasAr2:MR at 1516 cm^{-1} is much broader than that of QuasAr2:A1 (Figure S7C), most likely due to additional subcomponent bands at 1527, 1502 and 1479 cm^{-1} (Figure S7D). Interestingly, these correspond closely to those in QuasAr1:MR (1527, 1504 and 1479 cm^{-1}). Furthermore, like QuasAr1:MR, QuasAr2:MR exhibits a major increase in the intensity of the coupled HOOP mode assigned band at 964 cm^{-1} (Fig. 4b and Figure S9) indicating again an increased torsion around the single- and double-bond polyene system compared to QuasAr2:A1. This is further supported by the increased intensity of the isolated HOOP mode at 897 cm^{-1}.

We also considered the possibility that the 13-*cis* configuration in QuasAr2:A1/MR is due to a possible photoreaction occurring in the unphotolyzed state for example due to irradiation by the weak HeNe laser light (λ = 632 nm). However, this is unlikely since measurements made on BR purple membrane using the same FT-Raman instrument under the same conditions produced spectra characteristic of the dark-adapted BR similar to

earlier FT-Raman measurements on BR (49). In contrast, adding an external visible light results in spectra similar to light-adapted BR (data not shown). In addition, when QuasAr2:A1 is illuminated with the same external light (sufficient to keep BR light-adapted), no change in the FT-Raman spectrum was observed in comparison to the nonilluminated sample (Figure S10).

DISCUSSION

Bioengineering OTVSs to absorb in the near-infrared

Since the early work of Boyden and Deisseroth in 2005 (10–13), microbial rhodopsins have become important optogenetic tools for neuroscience researchers (50,51). A variety of microbial rhodopsins and their variants have been extensively used to photomodulate and photomonitor the cellular transmembrane potential (13,50). These include microbial rhodopsins found in all the major domains of life including archaebacteria, eubacteria, fungi and eukaryotic cells (50). One extremely useful class of microbial rhodopsins for controlling electrical activity are the algal-derived channelrhodopsins (52,53), which encompass both light-gated cation and anion channels (54–56).

An important advance in opsin-based optogenetics was the discovery of fluorescent opsin-based transmembrane voltage sensors (OTVSs) such as variants of GPR and AR3 (1,2). Directed evolution has led to improved versions of these OTVSs including QuasAr1 and QuasAr2 (5) and more recently Archon1 (57). Along with these, advances in fluorescence microscopy have enabled functional neural imaging in complex brain circuitry. For example, a fast volumetric wide-field fluorescence microscopic approach that extends the depth of field has recently enabled the 3D monitoring with high spatio-temporal resolution of large-scale ensembles of neuronal assemblies in living animals (58,59).

One limitation of the current generation of OTVS relates to the use of visible wavelengths to excite fluorescence emission. For example, tissue absorption and scattering limits the amount of exciting light that can reach deep regions of the brain, while scattering of the emitted light can cause blurring of images (60). In contrast, the NIR transparency window of tissues (referred to as the NIR optical window I) extends from 650 to 950 nm, where light scattering and absorption are dramatically reduced compared to visible light (9,60). In addition, NIR-absorbing OTVSs would reduce potential cross-talk excitation with red absorbing light-gated channelrhodopsins that have been used along with OTVSs to achieve all-optical electrophysiological patch clamping of neurons (5). Thus, NIR-absorbing and emitting microbial rhodopsins could provide a new window to measure deep brain neural activity with high spatio-temporal resolution in living animals without the use of invasive fiber optics.

The feasibility of engineering microbial opsins with both NIR absorbance and fluorescence was recently demonstrated using WT GPR and its mutants F234S and D212N/F234S, where the native A1 chromophore is substituted with the MMAR analog (14–16). The combination GPR-DNFS:MR shifts the absorption maximum over 200 nm into the NIR region (525 nm vs. 745 nm) and the fluorescence to ~ 820 nm (14). Since GPR does not express well in animal cells, similar MMAR substitution has been tested also in native AR3 and its mutant AR3-F229S (orthologous to GPR-F234S), which do express well. However, this resulted only in modest redshifts of 36 and 24 nm, respectively, but nevertheless in a strongly redshifted fluorescence peak at 815 nm (17). As a second example, substituting the native A1 chromophore of AR3 with a merocyanine retinal analog resulted in a substantial 200 nm redshift (absorption λ_{max} = 757 nm) when expressed in E. *coli*, but less redshifted emission (λ_{max} = 772 nm) than with MMAR (61).

Importantly, since all of the microbial rhodopsin MMAR analog pigments explored so far still function as light-driven proton pumps when their counterion has not been mutated (14,15,17), they may not be suitable as OTVSs since they can alter the membrane potential which is being measured. (Note that they may still function as suitable neural silencers if their pumping rate is sufficiently high.) In contrast, all of the OTVSs commonly in use such as AR3-D95N, QuasAr1, QuasAr2, and Archon1 do not exhibit light-driven proton pumping. This is most likely due to substitution of the Asp95 SB counterion, which also serves as the proton acceptor during the initial step in proton transport, with an Asn, His or Gln residue (2,5,57). Since all of these substituted residues at the SB counterion position are neutral, except at very low pH in the case of His, they also cause an intrinsic redshift of the absorption maximum as predicted by a simple point charge model of opsin color tuning (62). Thus, the combination of neutral counterions found in QuasArs and substitution with an MMAR chromophore with extended electron delocalization provides the potential for significant redshifting of both the absorption and fluorescence maxima without having the disadvantage of proton pump activity.

Although the present study does not yet establish that QuasAr:MRs can serve as effective OTVSs, which will require expression in animal cells combined with parallel optical and electrical measurements, several desirable features have emerged from our current study:

1 *Absorbance and excitation maxima reside in the NIR tissue transparency region*: The absorbance and excitation spectra of QuasAr1/2:MR fall well within the NIR tissue transparency region (650-950 nm), thereby strongly reducing light scattering and absorbance. In addition, the broadness of these bands allows fluorescence to be excited using NIR radiation (e.g. near 785 nm; Figure S5) causing minimal cross-talk with for example channelrhodopsins used to excite action potentials (such as ChR2 which absorbs near 480 nm).

2 *Less scattering and absorption of fluorescence:* The redshift from 715-730 nm to 830-850 nm for the maximum wavelength of fluorescence emission of QuasAr1/2:MR compared to QuasAr1/2:A1 (Fig. 3 and Figure S3) is favorable for their use as deep brain imaging OTVSs. In particular, the scattering of emitted light by tissue is strongly reduced at longer wavelengths. In addition, the Stokes shift is much larger compared to AR3 and variants regenerated with merocyanine retinal (61). For example, the largest Stokes shift reported for AR3 merocyanine analogs was for the AR3 mutant Mero-2, which was from 757 to 772 nm (61), much smaller than the over 140 nm Stokes shift reported here for QuasAR1/2:MR (see Figure S3).

3 *Increased Brightness of MMAR pigments*: The fluorescence results indicate that the analog QuasAr1/2:MR pigments are 5–10x brighter than the corresponding A1 pigments when using 600 nm excitation. Since 600 nm is much closer to the QuasAr1/2:A1 absorption maxima (~600 nm) than the QuasAr1/2:MR absorption maxima (~700 nm), the actual increase in

brightness is expected to be much larger when the MMAR analogs are excited at their excitation maxima. This conclusion is supported by earlier reports, from which it can be concluded that the fluorescence quantum yield measured for green proteorhodopsin containing the MMAR analog (GPR:MR) is 3-8 times higher (16) than that of QuasAr1/2:A1 (5).

The structure of the analog MMAR chromophore in QuasArs

The FT-Raman results show that the MMAR analog chromophore in QuasAr1 exists predominantly in an all-*trans* PSB configuration based on the characteristic bands appearing in the fingerprint region. However, the significant broadening of the main visible absorption band as well as the FT-Raman ethylenic band indicates that MMAR can adopt multiple iso-structures and/or possesses multiple electronic excitations pathways as discussed previously regarding MMAR contained in GPR and GPR-DNFS (14–16) and AR3 (17). The origin of these multiple forms/excitations is currently unknown. One possibility is variability in the electrostatic interactions between the PSB and the neutral His or Gln counterion. For example, a water molecule which is positioned between the counterion and PSB, as exists in BR (63) and some of its mutants such as D85N (64), might produce different subspecies with various absorption maxima if it existed in different structural configurations. Variability in the interaction with nearby residues such as Ser60 or Ser151 (see Fig. 5b) could also produce different subspecies (27). This is also exemplified by the strong enhancement of the NIR absorbance profile of GPR:MR by the F234S mutation (14). Alternatively, the broadening of the absorption might arise from multiple interactions of residues positioned near the methylamino group at the opposite end of the MMAR chromophore including Ser151 (see Fig. 5B). The methylamino group might contribute to resonance structures, with a *trans* as well as a *cis* conformation (14,16,17), e.g. Figure S1) causing different subspecies with different absorption profiles.

The existence of different resonance states of the MMAR chromophore is also likely to play an important role in the broadening of the absorption and ethylenic bands. For example, two resonant forms shown in Figure S11 are predicted to contribute to the absorption of GPR:MR at lower pH where the SB counterion (Asp97) is neutral due to protonation (see figure 4 from ref. (16)). These two resonance forms are also likely to play a role in QuasAr1/2:MR, since the His95 and Gln95 residues, respectively, are expected to exist in a neutral form. The second resonance form is likely to predominate in case negative or polar residues interact with the methylamino group such as S151 (see Figure 3 from Ref. (61)). Below pH 5, we observed a major shift in the ethylenic frequency in QuasAr1 (corresponding to a blueshift in the absorption). This can be attributed to protonation of the His95 counterion, which would significantly alter its interaction with the PSB and possibly a nearby H-bonded network including water molecules.

In the case of QuasAr2:A1/MR, we detect a chromophore which exists at least partially in a 13-*cis* isomeric state. Since the unphotolyzed state has properties similar to the O-intermediate of the BR photocycle, which is generally believed to exist in only an all-*trans* state (see below), this property might be thought to argue against this similarity. However, there is also evidence that the redshifted O-intermediate of the BR photocycle actually consists of two separate species, O(I), which exists in equilibrium with N and has a 13-*cis* chromophore, and O(II), where the chromophore has isomerized to an all-*trans* form and corresponds to the usually detected O-intermediate (65). In support of this model, two isomeric forms of O are detected in the BR mutant L93A, which has a significantly delayed late photocycle (66). In fact, the cryogenically trapped crystal structure of the O-intermediate of L93A reveals a 13-*cis*/15-*syn* form similar to dark-adapted BR but with a protein structure similar to the M-intermediate (67).

The existence of a 13-*cis* chromophore configuration associated with a neutral SB counterion has also been previously observed for several microbial rhodopsins in their unphotolyzed state. For example, an "acid blue" species in BR is generated between pH 2 and 3 due to protonation of the SB counterion Asp85 as well as in the BR mutant D85N due to the presence of a neutral Asn85 residue at the position of the
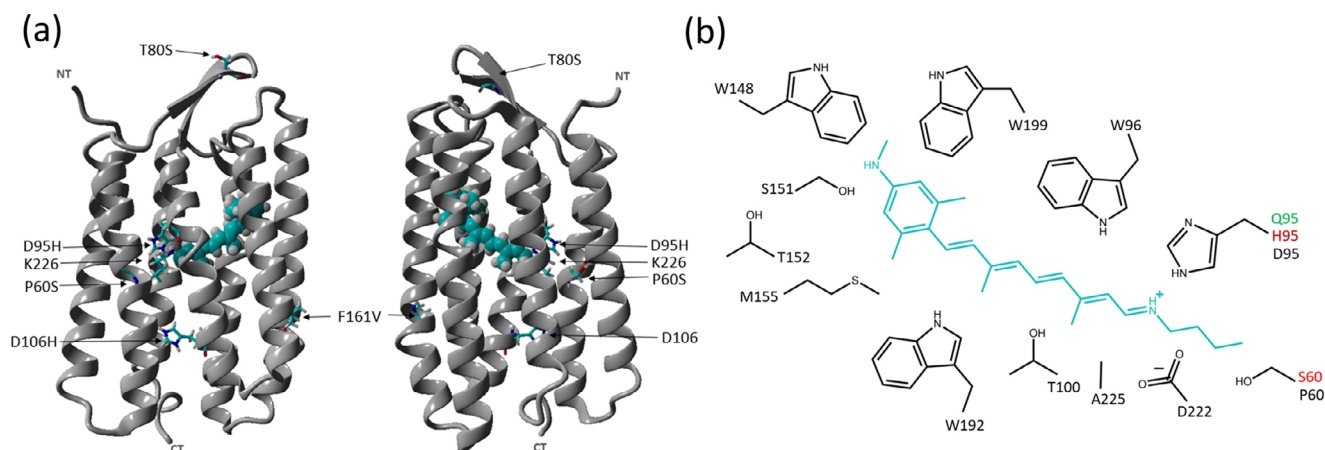

Figure 5. Homology model of QuasAr1 with MMAR chromophore. (a) Two different views rotated 180° around axis perpendicular to membrane plane of QuasAR1 with MMAR. Model was created and visualized using YASARA (www.yasara.org) as described in Materials and Methods. The mutation sites in QuasAr1 are shown in cyan as "stick model" of the side chains and the MMAR chromophore represented by a space filled molecule. (b) Schematic of selected side chains which surround the MMAR analog chromophore in the binding pocket with residues number shown in black for AR3 and substituted residues in QuasAr1 and QuasAr2 shown in red and green, respectively (adapted from (17)).

counterion. The A1 chromophore of both species exists as a mixture of all-*trans* and 13-*cis* isomers (64,68). As another example, in the mutant AR3-D95N (the homolog of BR-D85N), a 13-*cis* retinylidene isomer is detected which is enhanced at high pH, and also accumulates under high power 785-nm excitation (24).

Another conclusion from the present study is that more torsion exists in the polyene system of MR compared to A1 in QuasAr1/2 as indicated by intensification of the coupled HOOP modes near 963 cm^{-1} similar to previous observations in the O-photointermediate of the bacteriorhodopsin photocycle (38) and also GPR-DNFS:MR in its unphotolyzed state (15). Along with the extended resonant polyene system, such twisting could also contribute to the significant redshifts observed in the MMAR pigments.

In general, it is not surprising that the substitution of analog retinals for a native A1 chromophore produces unusual properties such as a transition to an O-like state normally observed only as a photoproduct or a mixture of all-trans and 13-cis configurations. Microbial rhodopsin structures have in most part evolved to accommodate the relatively relaxed all-*trans* retinal A1 chromophore. Analog chromophores can adopt, as in the case of MMAR, a more twisted conformation to fit into this binding pocket. Modifications in or around the Schiff base region are also expected to affect the C13 = C14 bond *cis-trans* equilibrium. Such experimental modifications can also additionally diversify functional properties, which can be further strengthened or steered by strategic protein engineering.

A number of previous studies have used synthetic retinal analogs and also protein engineering to modify the spectral and kinetic characteristics of rhodopsins including in the area of optogenetics (69). However, these studies have focused mainly upon channelrhodopsins and did not result in NIR-absorbing pigments. For example, one study utilized DMAR (a dimethylaminophenyl-retinal analog), which differs from MMAR in the lack of methyl groups at the aromatic ring and in the substitution of a hydrogen for an additional methyl group at the amino group (Figure S1) (69). This resulted in only modest redshifts (e.g. in the ChR2 variant H134R expressed in *C. elegans,* it shifts the λ_{max} from 480 to 520 nm, and in AR3 expressed in *C. elegans,* it shifts the λ_{max} from 568 to 580 nm). In the case of OTVSs, as discussed above, a NIR-absorbing pigment was produced with the merocyanine-like retinal analog substitution in AR3 (70). In general, combining a neutral SB counterion with an extended resonance-enhanced polyene retinal analog such as in the case of QuasAr1:MR and QuasAr2:MR offers a promising approach for engineering NIR-OTVSs. A variety of directed evolution methods such as robotic multidimensional directed evolution (24) could further refine this approach to optimize such NIR-OTVSs.

SUPPORTING INFORMATION

Additional supporting information may be found online in the Supporting Information section at the end of the article:

Figure S1. Chemical structure of native and analog retinals.

Figure S2. Absorption spectra from 250-850 nm of different QuasArs with the native A1 and analog MMAR chromophore.

Figure S3. Contour plots of emission (fluorescence) vs. excitation for different QuasArs.

Figure S4. Fluorescence emission spectra of QuasAr1/2:A1 (blue/purple) and QuasAr1/2:MR (green/red) in DDM micelles at pH 7.3 recorded with 600 nm excitation light.

Figure S5. Florescence emission spectrum of QuasAr1:MR excited by a 785 nm diode laser as function of laser power.

Figure S6. Inverse linear correlation plots between ethylenic frequency and visible absorption wavelength maximum for QuasArs with A1 and MMAR chromophores.

Figure S7. Curve fitted FT-Raman spectra of QuasARs in the ethylenic C = C stretch region.

Figure S8. Comparison of FT-Raman spectrum of QuasAr1:A1 (red) and QuasAr2:A1 (blue) at pH 7.3.

Figure S9. FT-Raman spectra of QuasArs at pH 7.3 with A1 and MMAR chromophores in the HOOP mode region.

Figure S10. Comparison of FT-Raman spectrum of QuasAr2:A1 at pH 7.3 with visible illumination on and off.

Figure S11. Two resonance forms of the MMAR chromophore predicted to exist in microbial rhodopsins with neutral counterions such as His95 above pH 5 (QuasAr1) and Gln95 (QuasAr2).

REFERENCES

1. Kralj, J. M., D. R. Hochbaum, A. D. Douglass and A. E. Cohen (2011) Electrical spiking in *Escherichia coli* probed with a fluorescent voltage-indicating protein. *Science* **333**, 345–348.

2. Kralj, J. M., A. D. Douglass, D. R. Hochbaum, D. Maclaurin and A. E. Cohen (2012) Optical recording of action potentials in mammalian neurons using a microbial rhodopsin. *Nat Methods* **9**, 90.

3. Xu, Y., P. Zou and A. E. Cohen (2017) Voltage imaging with genetically encoded indicators. *Curr Opin Chem Biol* **39**, 1–10.

4. Diester, I., M. T. Kaufman, M. Mogri, R. Pashaie, W. Goo, O. Yizhar, C. Ramakrishnan, K. Deisseroth and K. V. Shenoy (2011) An optogenetic toolbox designed for primates. *Nat Neurosci* **14**, 387–397.

5. Hochbaum, D. R., Y. Zhao, S. L. Farhi, N. Klapoetke, C. A. Werley, V. Kapoor, P. Zou, J. M. Kralj, D. Maclaurin, N. Smedemark-Margulies, J. L. Saulnier, G. L. Boulting, C. Straub, Y. K. Cho, M. Melkonian, G. K. Wong, D. J. Harrison, V. N. Murthy, B. L. Sabatini, E. S. Boyden, R. E. Campbell and A. E. Cohen (2014) All-optical electrophysiology in mammalian neurons using engineered microbial rhodopsins. *Nat Methods* **11**, 825–833.

6. Jin, L., Z. Han, J. Platisa, J. R. Wooltorton, L. B. Cohen and V. A. Pieribone (2012) Single action potentials and subthreshold electrical events imaged in neurons with a fluorescent protein voltage probe. *Neuron* **75**, 779–785.

7. Lin, J. Y. (2011) A user's guide to channelrhodopsin variants: features, limitations and future developments. *Exp Physiol* **96**, 19–25.

8. Lin, J. Y., P. M. Knutsen, A. Muller, D. Kleinfeld and R. Y. Tsien (2013) ReaChR: a red-shifted variant of channelrhodopsin enables deep transcranial optogenetic excitation. *Nat Neurosci* **16**, 1499–1508.

9. Chernov, K. G., T. A. Redchuk, E. S. Omelina and V. V. Verkhusha (2017) Near-infrared fluorescent proteins, biosensors, and optogenetic tools engineered from phytochromes. *Chem Rev* **117**, 6423–6446.

10. Boyden, E. S., F. Zhang, E. Bamberg, G. Nagel and K. Deisseroth (2005) Millisecond-timescale, genetically targeted optical control of neural activity. *Nat Neurosci* **8**, 1263–1268.

11. Deisseroth, K. (2011) Optogenetics. *Nat Methods* **8**, 26–29.
12. Boyden, E. S. (2015) Optogenetics and the future of neuroscience. *Nat Neurosci* **18**, 1200–1201.
13. Adamantidis, A., S. Arber, J. S. Bains, E. Bamberg, A. Bonci, G. Buzsaki, J. A. Cardin, R. M. Costa, Y. Dan, Y. Goda, A. M. Graybiel, M. Hausser, P. Hegemann, J. R. Huguenard, T. R. Insel, P. H. Janak, D. Johnston, S. A. Josselyn, C. Koch, A. C. Kreitzer, C. Luscher, R. C. Malenka, G. Miesenbock, G. Nagel, B. Roska, M. J. Schnitzer, K. V. Shenoy, I. Soltesz, S. M. Sternson, R. W. Tsien, R. Y. Tsien, G. G. Turrigiano, K. M. Tye and R. I. Wilson (2015) Optogenetics: 10 years after ChR2 in neurons–views from the community. *Nat Neurosci* **18**, 1202–1212.
14. Ganapathy, S., H. Venselaar, Q. Chen, H. J. M. de Groot, K. J. Hellingwerf and W. J. de Grip (2017) Retinal-based proton pumping in the near infrared. *J Am Chem Soc* **139**, 2338–2344.
15. Mei, G., N. Mamaeva, S. Ganapathy, P. Wang, W. J. DeGrip and K. J. Rothschild (2018) Raman spectroscopy of a near infrared absorbing proteorhodopsin: Similarities to the bacteriorhodopsin O photointermediate. *PLoS ONE* **13**, e0209506.
16. Hontani, Y., S. Ganapathy, S. Frehan, M. Kloz, W. J. de Grip and J. T. M. Kennis (2018) Strong pH-dependent near-infrared fluorescence in a microbial rhodopsin reconstituted with a red-shifting retinal analogue. *J Phys Chem Lett* **9**, 6469–6474.
17. Ganapathy, S., S. Kratz, Q. Chen, J. Hellingwerf, H. J. M. de Groot, K. J. Rothschild and W. J. de Grip (2019) Red-shifted and near-infrared active analog pigments based upon archaerhodopsin-3. *Photochem Photobiol* **95**, 959–968.
18. Bergo, V., J. J. Amsden, E. N. Spudich, J. L. Spudich and K. J. Rothschild (2004) Structural changes in the photoactive site of proteorhodopsin during the primary photoreaction. *Biochemistry* **43**, 9075–9083.
19. Furutani, Y., Y. Sudo, A. Wada, M. Ito, K. Shimono, N. Kamo and H. Kandori (2006) Assignment of the hydrogen-out-of-plane and -in-plane vibrations of the retinal chromophore in the K intermediate of pharaonis phoborhodopsin. *Biochemistry* **45**, 11836–11843.
20. Ikeda, D., Y. Furutani and H. Kandori (2007) FTIR study of the retinal Schiff base and internal water molecules of proteorhodopsin. *Biochemistry* **46**, 5365–5373.
21. Ogren, J. I., S. Mamaev, D. Russano, H. Li, J. L. Spudich and K. J. Rothschild (2014) Retinal chromophore structure and Schiff base interactions in red-shifted channelrhodopsin-1 from Chlamydomonas augustae. *Biochemistry* **53**, 3961–3970.
22. Ganapathy, S., O. Becheau, H. Venselaar, S. Frolich, J. B. van der Steen, Q. Chen, S. Radwan, J. Lugtenburg, K. J. Hellingwerf, H. J. de Groot and W. J. de Grip (2015) Modulation of spectral properties and pump activity of proteorhodopsins by retinal analogues. *Biochem J* **467**, 333–343.
23. Joh, N. H., A. Oberai, D. Yang, J. P. Whitelegge and J. U. Bowie (2009) Similar energetic contributions of packing in the core of membrane and water-soluble proteins. *J Am Chem Soc* **131**, 10846–10847.
24. Saint Clair, E. C., J. I. Ogren, S. Mamaev, D. Russano, J. M. Kralj and K. J. Rothschild (2012) Near-IR resonance Raman spectroscopy of archaerhodopsin 3: effects of transmembrane potential. *J Phys Chem B* **116**, 14592–14601.
25. Krebs, R. A., U. Alexiev, R. Partha, A. M. DeVita and M. S. Braiman (2002) Detection of fast light-activated H+ release and M intermediate formation from proteorhodopsin. *BMC Physiol* **2**, 5.
26. Sawatzki, G., R. Fischer, H. Scheer and F. Siebert (1990) *Fourier-transform Raman spectroscopy applied to photobiological systems*, Vol. **87**, pp. 5903–5906., U.S.A.Proceedings of the National Academy of Sciences
27. Rath, P., M. P. Krebs, Y. He, H. G. Khorana and K. J. Rothschild (1993) Fourier transform Raman spectroscopy of the bacteriorhodopsin mutant Tyr-185–>Phe: formation of a stable O-like species during light adaptation and detection of its transient N-like photoproduct. *Biochemistry* **32**, 2272–2281.
28. Bergo, V. B., M. Ntefidou, V. D. Trivedi, J. J. Amsden, J. M. Kralj, K. J. Rothschild and J. L. Spudich (2006) Conformational changes in the photocycle of Anabaena sensory rhodopsin: absence of the Schiff base counterion protonation signal. *J Biol Chem* **281**, 15208–15214.
29. Bergo, V., E. N. Spudich, J. L. Spudich and K. J. Rothschild (2002) A Fourier transform infrared study of Neurospora rhodopsin: similarities with archaeal rhodopsins. *Photochem Photobiol* **76**, 341–349.
30. Bergo, V., S. Mamaev, J. Olejnik and K. J. Rothschild (2003) Methionine changes in bacteriorhodopsin detected by FTIR and cell-free selenomethionine substitution. *Biophys J* **84**, 960–966.
31. Kajimoto, K., T. Kikukawa, H. Nakashima, H. Yamaryo, Y. Saito, T. Fujisawa, M. Demura and M. Unno (2017) Transient resonance raman spectroscopy of a light-driven sodium-ion-pump rhodopsin from indibacter alkaliphilus. *J. Phys. Chem. B* **121**, 4431–4437.
32. Fodor, S. P., R. Gebhard, J. Lugtenburg, R. A. Bogomolni and R. A. Mathies (1989) Structure of the retinal chromophore in sensory rhodopsin I from resonance Raman spectroscopy. *J Biol Chem* **264**, 18280–18283.
33. Rath, P., K. D. Olson, J. L. Spudich and K. J. Rothschild (1994) The Schiff base counterion of bacteriorhodopsin is protonated in sensory rhodopsin I: spectroscopic and functional characterization of the mutated proteins D76N and D76A. *Biochemistry* **33**, 5600–5606.
34. Rath, P., E. Spudich, D. D. Neal, J. L. Spudich and K. J. Rothschild (1996) Asp76 is the Schiff base counterion and proton acceptor in the proton-translocating form of sensory rhodopsin I. *Biochemistry* **35**, 6690–6696.
35. Kralj, J. M., E. N. Spudich, J. L. Spudich and K. J. Rothschild (2008) Raman spectroscopy reveals direct chromophore interactions in the Leu/Gln105 spectral tuning switch of proteorhodopsins. *J Phys Chem B* **112**, 11770–11776.
36. Krebs, R. A., D. Dunmire, R. Partha and M. S. Braiman (2003) Resonance Raman Characterization of Proteorhodopsin's Chromophore Environment. *J Phys Chem B* **107**, 7877–7883.
37. Smith, S. O., M. S. Braiman, A. B. Myers, J. A. Pardoen, J. M. L. Courtin, C. Winkel, J. Lugtenburg and R. A. Mathies (1987) Vibrational analysis of the all-trans-retinal chromophore in light-adapted bacteriorhodopsin. *J Am Chem Soc* **109**, 3108–3125.
38. Smith, S. O., J. A. Pardoen, P. P. J. Mulder, B. Curry, J. Lugtenburg and R. Mathies (1983) Chromophore structure in bacteriorhodopsin's O640 photointermediate. *Biochemistry* **22**, 6141–6148.
39. Smith, S. O., A. B. Myers, R. A. Mathies, J. A. Pardoen, C. Winkel, E. M. van den Berg and J. Lugtenburg (1985) Vibrational analysis of the all-trans retinal protonated Schiff base. *Biophys J* **47**, 653–664.
40. Rothschild, K. J., J. Andrew, W. J. DeGrip and H. E. Stanley (1976) Opsin structure probed by Raman spectroscopy of photoreceptor membranes. *Science* **191**, 1176–1178.
41. Rothschild, K. J. and N. A. Clark (1979) Anomalous amide i infrared absorption of purple membrane. *Science* **204**, 311–312.
42. Rothschild, K. J., W. A. Cantore and H. Marrero (1983) Fourier transform infrared difference spectra of intermediates in rhodopsin bleaching. *Science* **219**, 1333–1335.
43. Palings, I., E. M. M. van den Berg, J. Lugtenberg and R. A. Mathies (1989) Complete assignment of the hydrogen out-of-plane wagging vibrations of bathorhodopsin: chromophore structure and energy storage in the primary photoproduct of vision. *Biochemistry* **28**, 1498–1507.
44. Bovee-Geurts, P. H. M., J. Lugtenburg and W. J. DeGrip (2017) Coupled HOOP signature correlates with quantum yield of isorhodopsin and analog pigments. *Biochim Biophys Acta* **1858**, 118–125.
45. Smith, S. O., J. A. Pardoen, J. Lugtenburg and R. A. Mathies (1987) Vibrational analysis of the 13-cis-retinal chromophore in dark-adapted bacteriorhodopsin. *J Phys Chem* **91**, 804–819.
46. Fodor, S. P. A., J. B. Ames, R. Gebhard, E. M. M. Van den Berg, W. Stoeckenius, J. Lugtenburg and R. A. Mathies (1988) Chromophore structure in bacteriorhodopsin's N intermediate: implications for the proton-pumping mechanism. *Biochemistry* **27**, 7097–7101.
47. Braiman, M. S., O. Bousche and K. J. Rothschild (1991) Protein dynamics in the bacteriorhodopsin photocycle: submillisecond Fourier transform infrared spectra of the L, M, and N photointermediates. *Proc Natl Acad Sci USA* **88**, 2388–2392.
48. Bousche, O., M. Braiman, Y. W. He, T. Marti, H. G. Khorana and K. J. Rothschild (1991) Vibrational spectroscopy of bacteriorhodopsin mutants. Evidence that ASP-96 deprotonates during the M—N transition. *J Biol Chem* **266**, 11063–11067.
49. Rath, P., L. L. DeCaluwe, P. H. Bovee-Geurts, W. J. DeGrip and K. J. Rothschild (1993) Fourier transform infrared difference spectroscopy of rhodopsin mutants: light activation of rhodopsin causes hydrogen-bonding change in residue aspartic acid-83 during meta II formation. *Biochemistry* **32**, 10277–10282.

50. Zhang, F., J. Vierock, O. Yizhar, L. E. Fenno, S. Tsunoda, A. Kiani-anmomeni, M. Prigge, A. Berndt, J. Cushman, J. Polle, J. Magnuson, P. Hegemann and K. Deisseroth (2011) The microbial opsin family of optogenetic tools. *Cell* **147**, 1446–1457.

51. Deisseroth, K. (2015) Optogenetics: 10 years of microbial opsins in neuroscience. *Nat Neurosci* **18**, 1213–1225.

52. Ernst, O. P., P. A. Sanchez Murcia, P. Daldrop, S. P. Tsunoda, S. Kateriya and P. Hegemann (2008) Photoactivation of channel-rhodopsin. *J Biol Chem* **283**, 1637–1643.

53. Nagel, G., M. Brauner, J. F. Liewald, N. Adeishvili, E. Bamberg and A. Gottschalk (2005) Light activation of channelrhodopsin-2 in excitable cells of Caenorhabditis elegans triggers rapid behavioral responses. *Curr Biol* **15**, 2279–2284.

54. Sineshchekov, O. A., E. G. Govorunova, H. Li and J. L. Spudich (2015) Gating mechanisms of a natural anion channelrhodopsin. *Proc Natl Acad Sci USA* **112**, 14236–14241.

55. Govorunova, E. G., O. A. Sineshchekov, E. M. Rodarte, R. Janz, O. Morelle, M. Melkonian, G. K. Wong and J. L. Spudich (2017) The expanding family of natural anion channelrhodopsins reveals large variations in kinetics, conductance, and spectral sensitivity. *Sci Rep* **7**, 43358.

56. Yi, A., H. Li, N. Mamaeva, R. E. Fernandez De Cordoba, J. Lugtenburg, W. J. DeGrip, J. L. Spudich and K. J. Rothschild (2017) Structural Changes in an Anion Channelrhodopsin: Formation of the K and L Intermediates at 80 K. *Biochemistry* **56**, 2197–2208.

57. Piatkevich, K. D., E. E. Jung, C. Straub, C. Linghu, D. Park, H. J. Suk, D. R. Hochbaum, D. Goodwin, E. Pnevmatikakis, N. Pak, T. Kawashima, C. T. Yang, J. L. Rhoades, O. Shemesh, S. Asano, Y. G. Yoon, L. Freifeld, J. L. Saulnier, C. Riegler, F. Engert, T. Hughes, M. Drobizhev, B. Szabo, M. B. Ahrens, S. W. Flavell, B. L. Sabatini and E. S. Boyden (2018) A robotic multidimensional directed evolution approach applied to fluorescent voltage reporters. *Nat Chem Biol* **14**, 352–360.

58. Xiao, S., H. A. Tseng, H. Gritton, X. Han and J. Mertz (2018) Video-rate volumetric neuronal imaging using 3D targeted illumination. *Sci Rep* **8**, 7921.

59. Shain, W. J., N. A. Vickers, J. Li, X. Han, T. Bifano and J. Mertz (2018) Axial localization with modulated-illumination extended-depth-of-field microscopy. *Biomed Opt Express* **9**, 1771–1782.

60. Shi, L., L. A. Sordillo, A. Rodriguez-Contreras and R. Alfano (2016) Transmission in near-infrared optical windows for deep brain imaging. *J Biophotonics* **9**, 38–43.

61. Herwig, L., A. J. Rice, C. N. Bedbrook, R. K. Zhang, A. Lignell, J. K. B. Cahn, H. Renata, S. C. Dodani, I. Cho, L. Cai, V. Gradinaru and F. H. Arnold (2017) Directed evolution of a bright near-infrared fluorescent rhodopsin using a synthetic chromophore. *Cell Chem Biol* **24**, 415–425.

62. Honig, B., U. Dinur, K. Nakanishi, V. Balogh-Nair, M. A. Gawinowicz, M. Arnaboldi and M. G. Motto (1979) An external point-charge model for wavelength regulation in visual pigments. *J Am Chem Soc* **101**, 7084–7086.

63. Luecke, H., B. Schobert, H. T. Richter, J. P. Cartailler and J. K. Lanyi (1999) Structure of bacteriorhodopsin at 1.55 A resolution. *J Mol Biol* **291**, 899–911.

64. Rath, P., T. Marti, S. Sonar, H. G. Khorana and K. J. Rothschild (1993) Hydrogen bonding interactions with the schiff base of bacteriorhodopsin: resonance raman spectroscopy of the mutants D85N and D85A. *J Biol Chem* **268**, 17742–17749.

65. Toth-Boconadi, R., L. Keszthelyi and W. Stoeckenius (2003) Photoexcitation of the O-intermediate in bacteriorhodopsin mutant L93A. *Biophys J* **84**, 3857–3863.

66. Subramaniam, S., D. A. Greenhalgh, P. Rath, K. J. Rothschild and H. G. Khorana (1991) Replacement of leucine-93 by alanine or threonine slows down the decay of the N and O intermediates in the photocycle of bacteriorhodopsin: implications for proton uptake and 13-cis-retinal—all-trans-retinal reisomerization. *Proc Natl Acad Sci USA* **88**, 6873–6877.

67. Zhang, J., Y. Yamazaki, M. Hikake, M. Murakami, K. Ihara and T. Kouyama (2012) Crystal structure of the O intermediate of the Leu93->Ala mutant of bacteriorhodopsin. *Proteins* **80**, 2384–2396.

68. Smith, S. O. and R. A. Mathies (1985) Resonance Raman spectra of the acidified and deionized forms of bacteriorhodopsin. *Biophys J* **47**, 251–254.

69. AzimiHashemi, N., K. Erbguth, A. Vogt, T. Riemensperger, E. Rauch, D. Woodmansee, J. Nagpal, M. Brauner, M. Sheves, A. Fiala, L. Kattner, D. Trauner, P. Hegemann, A. Gottschalk and J. F. Liewald (2014) Synthetic retinal analogues modify the spectral and kinetic characteristics of microbial rhodopsin optogenetic tools. *Nat Commun* **5**, 5810.

70. Flytzanis, N. C., C. N. Bedbrook, H. Chiu, M. K. Engqvist, C. Xiao, K. Y. Chan, P. W. Sternberg, F. H. Arnold and V. Gradinaru (2014) Archaerhodopsin variants with enhanced voltage-sensitive fluorescence in mammalian and Caenorhabditis elegans neurons. *Nat Commun* **5**, 4894.